

**Linear analysis of incompressible Rayleigh-Taylor instability in solids**

A. R. Piriz\* and J. J. López Cela

*E.T.S.I. Industriales, Universidad de Castilla-La Mancha and Instituto de Investigaciones Energéticas, 13071 Ciudad Real, Spain*

N. A. Tahir

*GSI Helmholtzzentrum für Schwerionenforschung Darmstadt, Planckstrasse 1, 64291 Darmstadt, Germany*

(Received 27 May 2009; revised manuscript received 3 August 2009; published 6 October 2009)

The study of the linear stage of the incompressible Rayleigh-Taylor instability in elastic-plastic solids is performed by considering thick plates under a constant acceleration that is also uniform except for a small sinusoidal ripple in the horizontal plane. The analysis is carried out by using an analytical model based on the Newton second law and it is complemented with extensive two-dimensional numerical simulations. The conditions for marginal stability that determine the instability threshold are derived. Besides, the boundary for the transition from the elastic to the plastic regime is obtained and it is demonstrated that such a transition is not a sufficient condition for instability. The model yields complete analytical solutions for the perturbation amplitude evolution and reveals the main physical process that governs the instability. The theory is in general agreement with the numerical simulations and provides useful quantitative results. Implications for high-energy-density-physics experiments are also discussed.

DOI: [10.1103/PhysRevE.80.046305](https://doi.org/10.1103/PhysRevE.80.046305)

PACS number(s): 47.20.-k, 46.90.+s, 52.57.Fg

**I. INTRODUCTION**

Rayleigh-Taylor instability (RTI) is of central importance in the design of several experiments on high-energy density physics as well as in some fundamental problems in other branches of physics. However, in contrast to the classical case involving Newtonian or ideal fluids [1,2], RTI in accelerated solids is still poorly understood, although it has been a subject of research for more than forty years [3–17]. The difficulties for constructing a compelling theory of the linear growth phase of the RTI in solids have been essentially due to the character of the elastic-plastic constitutive properties of a solid which have a nonlinear dependence on the magnitude of the rate of deformation [18].

The present work is mainly motivated by the design requirements of one of the most interesting experiments planned in the framework of the facility for antiproton and ion research (FAIR) that is under construction at the GSI Helmholtzzentrum für Schwerionenforschung Darmstadt in Germany [19]. This experiment called LAPLAS (Laboratory of Planetary Sciences) is directed to the study of equation of state (EOS) and transport properties of high-energy density matter (HEDM) by using a low entropy cylindrical implosion driven by an intense heavy ion beam [20–23]. An RF-wobbler will be used to rotate the beam to generate a ring shaped focal spot in order to heat the annular region (the absorber) that surrounds a pusher made of a heavy metal. This pusher is imploded by the absorber expansion and compresses a material sample placed in the axial region of the cylindrical target. The wobbler system rotating the ion beam will generate an azimuthal asymmetry [24,25] that can seed the hydrodynamic instabilities at the absorber/pusher interface converting it in an issue of possible concern since the instabilities could spoil the performance of the implosion.

A similar problem is present in other experiments involving cylindrical implosions driven by different means such as

in the case of liners imploded by intense electrical currents delivered by pulsed power machines [26]. On the other hand, RTI in solids is also of relevance to some industrial applications such as explosive welding [27] as well as in other experiments on HEDM in which metallic plates are accelerated by means of high explosives [5,6] or laser beams [28–30]. In particular, accelerated metallic plates indirectly driven by an intense laser pulse are currently used to infer solid material strength by direct measurements of the RTI growth of initial perturbations performed on the plate surface [28–31]. In addition, RTI in solids is central to geophysics as it plays a role in the thickening of the cold and dense lithosphere beneath mountain belts [32,33]. In astrophysics, RTI in elastic solids is considered to be at the origin of the gamma-bursts produced by some slowly accreting neutron stars with a magnetosphere in which the accreted layer becomes denser than the underlying crust. The energy released during the overturn of the unstable interface excites the magnetosphere producing a gamma burst [34].

The physics of RTI in solids is essentially determined by the elastic-plastic properties of the material which present a series of complex phenomena that has not been understood so far despite of the long history of research on this subject. The first study was performed by Miles [3] by developing an approximate model based on an energy balance equation that was later used by several authors [4,9,12]. The Miles approach, known as a one-degree-of-freedom model, gives a qualitative picture of the instability but it considerably underestimates the asymptotic growth rate for pure elastic materials and, more importantly, it fails to give a description of the transition from the regime in which instability is dominated by the elastic properties to the regime in which it is controlled by the plastic properties. In 1974, Barnes *et al.* [5] conducted the first experimental study of RTI in aluminum plates accelerated by explosives. In 1980, Drucker [10,11] suggested that in some of the Barnes experimental results the evolution of the perturbations was controlled by the initial perturbation amplitude rather than by the perturbation wavelength. This was confirmed in later experiments by Barnes *et*

\*roberto.piriz@uclm.es

*al.* [6] and it was also evidenced in the extensive two-dimensional (2D) simulations performed by Sweigle and Robinson [8]. An intense research activity including approximate modeling, numerical simulations and experiments was also carried out in the former USSR and it was compiled in a report available in English in 1997 [17]. In this report, an approximate analytical model is developed for very thin plates with perfectly elastic properties and its results are extrapolated in a phenomenological manner to plates of arbitrary thickness.

The only exact theoretical analyses that are available have been performed for the simplest case of perfectly elastic (Hookean) solids [35,36]. The study by Plohr and Sharp [35] considered the RTI problem in accelerated plates of infinite extent but with arbitrary thickness and it was restricted to solid/vacuum interfaces. In the more recent work by Terrones [36], exact solutions are obtained for arbitrary Atwood numbers (solid/solid and solid/liquid interfaces) but it is restricted to infinite thickness media and, since this study is based on a normal modes analysis, it only describes the asymptotic behavior of the instability. That is the initial transient phase which is essential for determining the transition from the elastic to the plastic regime is not treated.

Despite the limitations of these exact theories, they are of great value as they allow for testing more general albeit approximate models (including numerical simulations) that may be necessary in order to deal with complex physical situations for which the approaches taken in those theories are not suitable. In fact, so far these approaches have shown to be too involved for admitting extensions that can include the most important aspect present in RTI in solids as it is the transition to the plastic regime. The simplest one-degree-of-freedom models based on an energy balance equation [3,4,9,12] can certainly include more realistic physics but as we have already mentioned, they do not allow for constructing satisfactory models. In Refs. [37–39] we have developed an approach based on the Newton second law that for the case of perfectly elastic solids produced analytical results in excellent agreement with the exact theories of Refs. [35,36] converting it into the best candidate for the construction of a relatively simple, nevertheless accurate model of the RTI in elastic-plastic solids.

In this work we develop such a model and we come up with a stability criterion that shows that transition to a plastic regime is a necessary but not a sufficient condition for instability as it was erroneously assumed in Refs. [15–17]. We have recently communicated the fundamentals of the model in Ref. [40]. In this paper we present complete account of the model by obtaining the explicit analytical solutions that describes the evolution of the perturbation amplitude. We have also completed the study with extensive 2D numerical simulations performed with the finite element code ABAQUS [41].

Under realistic conditions, pure RTI cannot be observed from the beginning of the plate acceleration process. When the pressure accelerating the plate rises up to its maximum value  $p_0$ , a shock wave or a weak compression wave is launched into the plate transporting the initial corrugations on the front surface to the plate rear side while the perturbation at the front face increases as a consequence of a

Ritchmyer-Meshkov-like instability. During the process the incident compression wave is reflected as a rarefaction wave and this sequence of compression and expansion waves is repeated several times until the plate becomes accelerated uniformly, provided that the pressure is not varying too fast. It is at this moment when the perturbations can be considered to evolve as a consequence of pure RTI but it will happen by taking new “initial” conditions that are settled by the previous sequences of compression and expansion waves. The previous mechanism, for which the new initial conditions for the growth of RTI are imposed, is known as RTI seeding, and although that it is not yet completely understood, it is a well-known problem in gas dynamics [42–46]. However, when it was observed by Sweigle and Robinson [8] in their 2D numerical simulations of solid plates accelerated by a ramp pressure, they were driven to the wrong conclusion that they were dealing with a new kind of instability that was a characteristic of accelerated solids with no equivalent in fluid dynamics. Actually, the general kinematics of the continuous media are the same either for solids and fluids except only by the different constitutive models necessary for describing the different media [47].

Here, we have performed our analysis by clearly defining the physical situation in order to study the linear phase of growth of pure incompressible RTI in thick plates ( $kh \gg 1$ ,  $k = 2\pi/\lambda$  is the perturbation wave number and  $h$  is the plate thickness) under a constant and uniform acceleration  $g$ .

## II. ANALYTICAL MODEL

### A. Fundamental equations

In order to construct the model we have assumed a uniform and incompressible solid plate of density  $\rho$  with elastic-plastic constitutive properties which is sufficiently thick ( $kh \gg 1$ ) so that finite thickness effects can be neglected and it can be considered as occupying the half-space  $y < 0$ . It is assumed that the plate has been accelerated for a very long time until the time  $t=0$  by a constant and uniform pressure  $p_0$  that represents a low density ideal fluid accelerating the plate with an acceleration  $\vec{a} = -g\mathbf{e}_y$  ( $g = p_0/\rho h$ ). At  $t=0$ , a ripple  $\delta p = -p_0(\xi_0/h)e^{ky} \sin kx$  is superposed to the uniform pressure  $p_0$ . The alternative approach of taking a uniform pressure that accelerates a plate with preformed corrugations of amplitude  $\xi_0$  is entirely equivalent from the analytical point of view but as it will be explained later, in practice, it is more difficult to realize in our numerical simulations so that in order to make the comparisons, we adopt the approach of considering a rippled driving pressure. On the other hand, the latter is just the situation relevant to the LAPLAS experiment where the pressure ripple will be created by the rotating beam [24,25].

Nevertheless, as we will show below, equations are easily transformed from one to the other approach just by a simple change of variables. Then with our rippled pressure choice, the equation of motion for describing the linear evolution of the perturbation amplitude in the vertical direction turns out [37–39] (see the Appendix):

$$\frac{\rho}{k} \ddot{\eta} = \rho g (\eta + \eta_0) - S_{yy}, \quad (1)$$

with the following initial conditions:

$$\eta(0) = 0; \quad \dot{\eta}(0) = 0, \tag{2}$$

where  $\rho/k$  is the mass per unit area within the region of thickness  $k^{-1}$  and it is the only mass of the plate that participates in the motion caused by the instability. In addition,  $S_{yy}$  is the normal component of the perturbation of the deviatoric part  $S_{ij}$  of the stress tensor  $\sigma_{ij} = -p\delta_{ij} + S_{ij}$  ( $p$  is the thermodynamic pressure and  $\delta_{ij}$  is the Kronecker tensor). Here and in the rest of this work, we use the usual index tensor notation where  $i$  and  $j$  denote coordinate directions ( $i, j = x, y, z$ ) and repeated index will denote summation. On the other side, following previous works [37,38], we assume that the velocity field can be approximated by the one corresponding to an ideal inviscid fluid:

$$v_x = \dot{\xi}(t)e^{ky} \cos kx; \quad \dot{\eta} = v_y = \dot{\xi}(t)e^{ky} \sin kx, \tag{3}$$

where  $\xi(t)$  is the instantaneous perturbation amplitude on the interface ( $y=0$ ). Therefore, we have

$$\eta = \xi(t)e^{ky} \sin kx. \tag{4}$$

In the alternative case of considering perturbations on the plate surface and a uniform driving pressure, the corresponding equation of motion is obtained by replacing  $\eta' = \eta + \eta_0$  by  $\eta$ .

Solving Eq. (1) requires to obtain a convenient expression for the tensor  $S_{ij}$ . For this we assume the nonlinear Prandtl-Reuss model with the von Mises yield stress criterion which provides the following differential equations for the components of the deviatoric tensor  $S_{ij}$  [9,18]:

$$\dot{S}_{ij} = 2GD_{ij} \tag{5}$$

if

$$S_{ij}D_{ij} < 0 \text{ or } S_{ij}S_{ij} < \frac{2}{3}Y^2, \tag{6}$$

and

$$\dot{S}_{ij} + 2GS_{ij} \frac{S_{mn}D_{mn}}{S_{mn}S_{mn}} = 2GD_{ij} \tag{7}$$

if

$$S_{ij}D_{ij} > 0 \text{ and } S_{ij}S_{ij} = \frac{2}{3}Y^2 \tag{8}$$

where  $G$  is the shear modulus,  $Y$  is the yield strength, and both are parameters characteristic of the solid material. To the scope of a parametric study they will be taken as independent parameters [8,9]. Besides, in Eqs. (5)–(8),  $D_{ij}$  is the rate of deformation tensor which for an incompressible medium reads

$$D_{ij} = \frac{1}{2} \left( \frac{\partial v_i}{\partial x_j} + \frac{\partial v_j}{\partial x_i} \right). \tag{9}$$

The previous differential equations for  $S_{ij}$  can be solved as in Ref. [4] (see also Ref. [9]). Let us briefly summarize the main steps to get the solution. First, for convenience we define the time-independent tensor  $M_{ij}$  as in Ref. [9]:

$$M_{ij} = \frac{D_{ij}}{k\dot{\xi}}. \tag{10}$$

Then, for  $|S| < \sqrt{2/3}Y$  or  $S_{ij}D_{ij} < 0$  ( $k\dot{\xi} < 0$ ) we have to take Eq. (5). We multiply it by  $D_{ij}$  and using Eq. (10) we get, after integration with the condition  $S_{ij}(\eta=0)=0$ :

$$S_{ij} = 2kGM_{ij}\xi; \quad \text{if } |S| < \sqrt{\frac{2}{3}}Y. \tag{11}$$

Proceeding in the same manner with Eq. (7), for  $S_{ij}D_{ij} > 0$  ( $k\dot{\xi} > 0$ ) and  $|S| = \sqrt{2/3}Y$ , we get the following expression for the product  $S_{ij}M_{ij}$  [9,44]:

$$\Phi(\bar{x}) = \frac{\Phi_0 + \tanh(\bar{x} - \bar{x}_0)}{1 + \Phi_0 \tanh(\bar{x} - \bar{x}_0)}. \tag{12}$$

where the following dimensionless variables has been defined:

$$\Phi = \frac{S_{ij}M_{ij}}{|M|\sqrt{\frac{2}{3}}Y}, \quad \bar{x} = \frac{2kG|M|}{\sqrt{\frac{2}{3}}Y}\xi. \tag{13}$$

Presenting Eq. (12) into Eq. (7) we get the differential equation for  $S_{ij}$  [44]:

$$\frac{dS}{d\bar{x}} + \Phi(\bar{x})S = 1, \quad S(\bar{x}_0) = S_0, \tag{14}$$

where we have defined  $S$  as

$$S = \frac{|M|}{\sqrt{\frac{2}{3}}YM_{ij}}S_{ij}. \tag{15}$$

Since across the yield surface (where  $|S| = \sqrt{2/3}Y$ )  $S_{ij}$  must be continuous, it turns out that  $S=1$  and, therefore, we have [44]

$$S_{ij} = \sqrt{\frac{2}{3}} \frac{M_{ij}}{|M|} Y; \quad \text{if } k\dot{\xi} > 0 \text{ and } |S| = \sqrt{\frac{2}{3}}Y. \tag{16}$$

The auxiliary tensor  $M_{ij}$  in Eqs. (11)–(16) can be calculated by using the assumed velocity field given by Eq. (3):

$$M_{yy} = -M_{xx} = e^{ky} \sin kx; \quad M_{xy} = e^{ky} \sin kx. \tag{17}$$

Therefore  $|M| = \sqrt{2}e^{ky}$  and the normal component  $S_{yy}$  of the deviatoric part of the stress tensor turns out:

$$S_{yy} = \begin{cases} 2kG\xi e^{ky} \sin kx & \text{if } \xi \leq \xi_p \\ \frac{1}{\sqrt{3}}Y \sin kx & \text{if } \xi \geq \xi_p, \end{cases} \tag{18}$$

where  $\xi_p$  denotes the perturbation amplitude at the interface ( $y=0$ ) at the time when the transition from the elastic to the plastic regime takes place. The previous expression applies if  $k\dot{\xi} \geq 0$ . If it becomes  $k\dot{\xi} < 0$ , the material relaxes and comes back to the elastic regime with the new initial conditions left by the previous plastic phase.

Using the expression for  $S_{yy}$  given by Eq. (18) and  $\eta$  given by Eq. (4), Eq. (1) yields the equation of motion of the interface. Since all the terms in Eq. (1) are proportional to

sin  $kx$ , we get an equation that is independent of the  $x$  coordinate. Instead, since the plastic branch of Eq. (18) is independent of the  $y$  coordinate, the equation derived from Eq. (1) depends on  $y$ . According to Eq. (18) the onset of plastic flow occurs first at  $y=0$  where deformation is a maximum and as the perturbation grows the plastified region progresses toward the plate interior. Since in RTI we have to deal with the average motion of a region affected by the instability which extends up to a distance of the order of  $k^{-1}$  from the interface, the onset of the plastic flow is not expected to be felt until plastic flow has affected the entire region with thickness of the order of  $k^{-1}$ . In this sense, it is not necessary that Eq. (18) gives a precise account of the spatial distribution of  $S_{yy}$  at the plate interior which probably is much more complex, but it is just enough that it gives a reasonable approximation of its average behavior over the region of thickness  $k^{-1}$  [37,38]. Therefore, we evaluate Eq. (1) at  $y=y_p \approx -k^{-1}$  and we get

$$\ddot{\xi} = \begin{cases} kg(\xi + \xi_0) - 2k^2G\xi/\rho & \text{if } \xi \leq \xi_p \\ kg(\xi + \xi_0) - \alpha Yk/\rho\sqrt{3} & \text{if } \xi \geq \xi_p, \end{cases} \quad (19)$$

where  $\xi_p = \alpha Y/2\sqrt{3}kG$  with  $\alpha = e^{k|y_p|} \approx e$  and it is taken  $\alpha=3$  in order to get a better fit with the numerical simulation results. This equation must be solved with the following initial conditions:  $\xi(0)=0$  and  $\dot{\xi}(0)=0$ .

For progressing further it is convenient to present the following dimensionless magnitudes:

$$z = \frac{\xi}{\xi_0}, \quad \tau = t\sqrt{kg}, \quad \hat{\lambda} = \frac{\rho g \lambda}{4\pi G}, \quad \hat{\xi} = \frac{\rho g \xi_0}{\sqrt{3}Y}. \quad (20)$$

Then, Eq. (19) reads

$$\ddot{z} = \begin{cases} z(1 - \hat{\lambda}^{-1}) + 1 & \text{if } z \leq z_p \\ z + 1 - \hat{\xi}^{-1} & \text{if } z \geq z_p, \end{cases} \quad (21)$$

$$z_p = \frac{\hat{\lambda}}{\hat{\xi}}, \quad (22)$$

and the corresponding initial conditions are:  $z(0)=0$  and  $\dot{z}(0)=0$ . Equation (21) can be explicitly solved to yield the complete evolution of the amplitude in the linear phase. However, before proceeding to study the analytic solutions of this equation, let us first discuss the stability boundaries.

### B. Instability threshold

We can extract important implications for the instability condition from the equation of motion of the interface by considering Eq. (21) together with its first integral:

$$\dot{z}^2 = \begin{cases} z^2(1 - \hat{\lambda}^{-1}) + 2z & \text{if } z \leq z_p \\ (z + 1 - \hat{\xi}^{-1})^2 - C^2/\hat{\xi}^2 & \text{if } z \geq z_p, \end{cases} \quad (23)$$

$$C^2 = (1 - \hat{\xi})^2 - \hat{\lambda}, \quad (24)$$

where we have taken into account the initial condition  $\dot{z}(0)=0$ .

From Eqs. (21) and (23) we get the instability threshold by noting that if the interface is stable the amplitude  $z(\tau)$  must have a maximum at a certain time  $\tau = \tau_m$ . This implies one must have  $\dot{z}(\tau_m)=0$  and  $\ddot{z}(\tau_m) \leq 0$  in order to assure that the extreme is actually a maximum. Instead, if it is  $\ddot{z}(\tau_m) \geq 0$ , the extreme will be an inflection point and the interface will be unstable. Therefore, the conditions for marginal stability that determine the instability threshold reads

$$\dot{z}(\tau_m^{TH}) = 0; \quad \ddot{z}(\tau_m^{TH}) = 0. \quad (25)$$

It is seen from Eqs. (21)–(24) that the previous marginal stability conditions are never satisfied for  $\hat{\lambda} > 1$ , and neither for  $\hat{\lambda} \leq 1$  if  $z \leq z_p$ . In fact, as in the case of a perfectly elastic solid, the interface is unstable for  $\hat{\lambda} > 1$  [35–37]. In this case, as we will see in the next subsection, the perturbation amplitude grows as in the case of a perfectly elastic solid until the elastic limit is achieved and then it continues to grow in the regime controlled by the plastic flow. Instead, for  $\hat{\lambda} < 1$ , for which the interface was found to be always stable in the perfectly elastic case [35–37], we can see in this case that it can be unstable or stable depending on the value of the dimensionless perturbation amplitude  $\hat{\xi}$ . For this, we apply the conditions for marginal stability given by Eq. (25) (for  $z \geq z_p$ ) and we find the following expression for the instability threshold:

$$\hat{\xi}_{TH} = 1 - \sqrt{\hat{\lambda}}. \quad (26)$$

That is, the interface will be unstable if  $\hat{\xi} > \hat{\xi}_{TH}$ . In dimensional magnitudes we have

$$\left(\frac{\rho g \xi_0}{\sqrt{3}Y}\right)_{TH} = 1 - \sqrt{\frac{\rho g \lambda}{4\pi G}}. \quad (27)$$

It is worth noticing here that since the conditions for marginal stability given by Eq. (25) can only be satisfied for  $z \geq z_p$ , the instability threshold lies always beyond the elastic limit where the transition from the elastic to the plastic regime occurs (EP transition). We can also obtain such a boundary for the EP transition by requiring that the maximum perturbation amplitude  $z_m^e = 2\hat{\lambda}/(1 - \hat{\lambda})$  in the pure elastic regime given by Eq. (23) (for  $z \leq z_p$ ,  $\hat{\lambda} < 1$ ) be equal to the amplitude  $z_p = \hat{\lambda}/\hat{\xi}$  which is the necessary to reach the elastic limit. Thus, the condition for the EP transition turns out to be

$$\hat{\xi}_{EP} = \frac{1}{2}(1 - \hat{\lambda}), \quad (28)$$

or in dimensional magnitudes one can write

$$\left(\frac{\rho g \xi_0}{\sqrt{3}Y}\right)_{EP} = \frac{1}{2} \left(1 - \frac{\rho g \lambda}{4\pi G}\right). \quad (29)$$

As one can see, since the EP transition occurs always before the achievement of the instability threshold, transition to the plastic regime is a necessary condition for instability. However, it is not at all a sufficient one. This result is in contrast to the assumption of Refs. [15–17] where EP transition was erroneously identified with instability that on the other side, was actually derived for thin plates ( $kh \ll 1$ ) and extrapolated to arbitrary thick plates.

It may be important to emphasize that, as we have already mentioned, the RTI is governed by the bulk motion of the mass contained within a region of thickness of the order of  $k^{-1}$  and therefore, the boundary for the EP transition is not determined by the onset of the plastic flow at any particular material point of the plate. Rather, it is the achievement of the elastic limit over the extended region affected by the instability what actually determines the transition from a regime in which the instability is controlled by the elastic properties to the one in which it is controlled by the plastic material properties. So the condition for the onset of plastic flow at the interface ( $y=0$ ) calculated in Ref. [48] by using the exact theory of Ref. [35] has no special relevance for the stability analysis. For the same reason, such a local condition cannot be compared with Eq. (29) in our paper.

In Fig. 1 we have represented the instability threshold given by Eq. (27) [curve (a)] and the EP transition boundary given by Eq. (29) [curve (b)] together with the EP transition boundary [curve (c)] derived in Refs. [15–17] (which was confused with the instability threshold). In the same figure we also show the instability threshold for a perfectly elastic solid which is given by the condition  $\hat{\lambda} < 1$  [curve (d)]. We also show the instability threshold for a perfectly rigid plastic solid derived by Drucker [10,11] [line (e)]. As one can appreciate the Drucker threshold is lower than our upper limit (for  $\hat{\lambda}=0$ ) by a factor of  $\sqrt{3}/2$ . An interesting connection between the present results and the Drucker criterion can be made by calculating the perturbation amplitude  $z_m^{TH} = z(\tau_m^{TH})$  just on the instability threshold:

$$z_m^{TH} + 1 = \frac{1}{\hat{\xi}_{TH}} = \frac{1}{1 - \sqrt{\hat{\lambda}}}, \quad (30)$$

where for writing the second equality we have used Eq. (26). In dimensional magnitudes it reads:

$$z(\tau) = \begin{cases} \frac{\hat{\lambda}}{1 - \hat{\lambda}}(1 - \cos \gamma\tau), & \tau \leq \tau_p \\ \frac{1}{\hat{\xi}} - 1 + \frac{C^2 e^{-(\tau - \tau_p)}}{2\hat{\xi}(u_p + \sqrt{u_p^2 - C^2})} + \frac{(u_p + \sqrt{u_p^2 - C^2})e^{-(\tau - \tau_p)}}{2\hat{\xi}}, & \tau_p \leq \tau \leq \tau_m \\ \frac{1 - C}{\hat{\xi}} - 1 - [1 - A \cos \gamma(\tau - \tau_m)], & \tau \geq \tau_m, \end{cases} \quad (32)$$

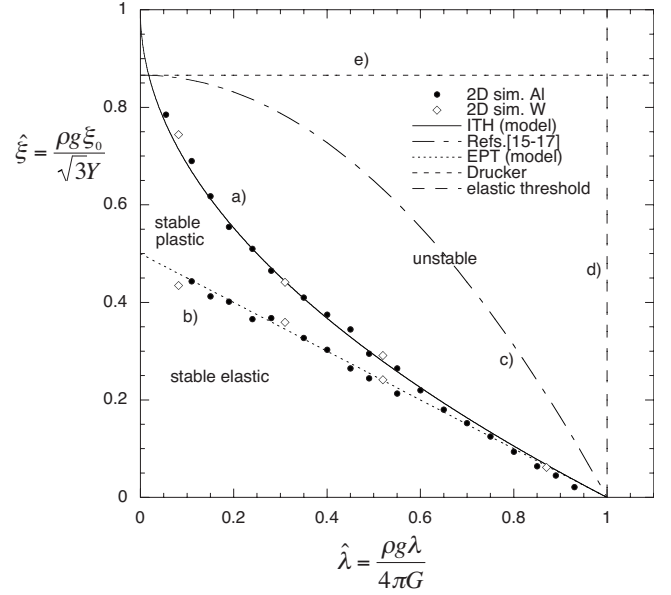


FIG. 1. Dimensionless amplitude  $\hat{\xi}$  as a function of the dimensionless perturbation wavelength  $\hat{\lambda}$  for the instability threshold and for the EP transition boundary.

$$\frac{\rho g(\xi_m^{TH} + \xi_0)}{\sqrt{3}Y} = 1. \quad (31)$$

Except by the factor  $\sqrt{3}/2$ , this equation reduces to the Drucker criterion for  $\hat{\lambda}=0$  when no perturbation grow occurs and  $\xi_m=0$ . Generally speaking, Eq. (31) shows that instability occurs when the pressure difference  $\rho g(\xi_m^{TH} + \xi_0)$  across a crest (or a valley) becomes larger than  $\sqrt{3}Y$ . That is, in general this relationship is not valid over the initial perturbation amplitude as Drucker [10,11] assumed, but rather it applies to the actual amplitude of the perturbation when it achieves the instability threshold. This condition also resembles the one usually considered to estimate the maximum possible high of a mountain either on Earth or on a neutron star [49].

### C. Analytical solutions

The complete analytical solutions of Eq. (21) can be obtained upon integration of this equation to yield the evolution of the perturbation amplitude. Stable solutions only exist for  $\hat{\lambda} \leq 1$  and  $C^2 \geq 0$ :

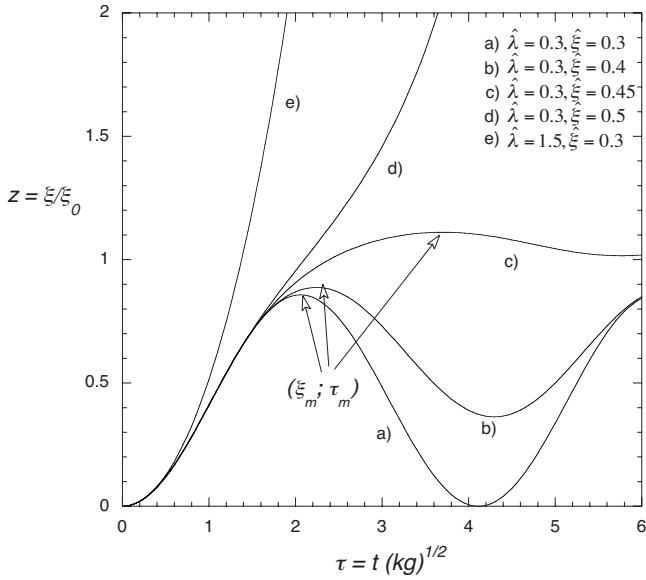


FIG. 2. Perturbation amplitude as a function of time for different values of the dimensionless amplitude  $\hat{\xi}$  and of the dimensionless wavelength  $\hat{\lambda}$ .

where the following definitions have been used:

$$\gamma = \sqrt{\frac{1-\hat{\lambda}}{\hat{\lambda}}}; \quad \tau_p = \frac{1}{\gamma} \arccos\left(\frac{u_p}{\hat{\xi}}\right); \quad u_p = \hat{\xi} - 1 + \hat{\lambda};$$

$$A = \frac{\hat{\lambda}C}{\hat{\xi}(1-\hat{\lambda})}; \quad \tau_m = \tau_p + \frac{1}{2} \ln \left[ \frac{C^2}{\hat{\xi}} (u_p + \sqrt{u_p^2 - C^2}) \right]. \quad (33)$$

These stable solutions correspond to conditions that would also give stable solutions in the case of perfectly elastic solids. However, for the present case of elastic-plastic solids, Eq. (32) yields two kinds of stable behavior. One of them corresponds to pure elastic oscillations in which the maximum amplitude remains always below the boundary of the EP transition. The other one, instead, corresponds to the case in which the elastic limit is overcome, the solid enters in the plastic regime (for  $\tau \geq \tau_p$ ) and the amplitude reaches the maximum at  $\tau = \tau_m$ . After this maximum, the system enters

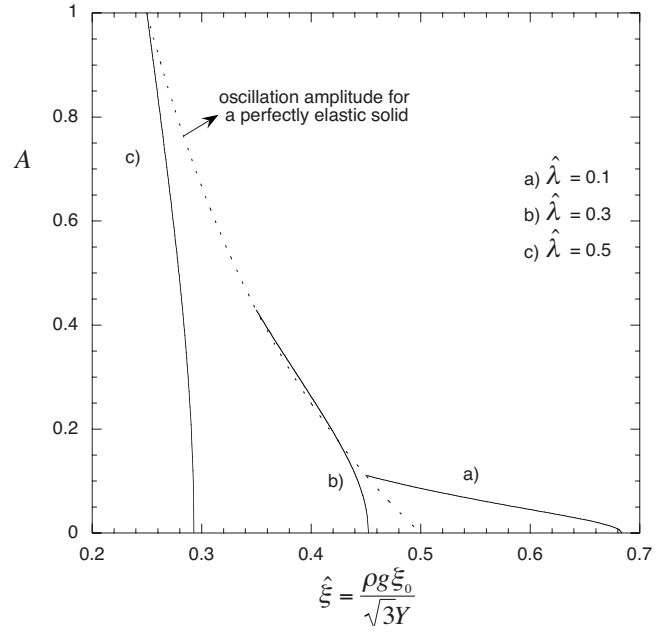


FIG. 3. Amplitude  $A$  of the elastic oscillations as a function of the dimensionless perturbation amplitude  $\hat{\xi}$  for several values of the dimensionless wavelength  $\hat{\lambda}$ . The amplitudes for the minimum values of  $\hat{\xi}$  correspond to a perfectly elastic solid (dotted line).

again in an elastic regime starting with the new conditions left at  $\tau_m$  by the previous plastic phase. These two kinds of stable solutions are shown in Fig. 2 where curve (a) is for the perfectly elastic case, and (b) and (c) are two examples for which the perturbation amplitude remains oscillating elastically after a period of time in which it grows in the plastic regime ( $\tau_p \leq \tau \leq \tau_m$ ). In the latter cases, the amplitude of the oscillations decreases from the value  $z_m^e/2 = \hat{\lambda}/(1-\hat{\lambda})$  for the perfectly elastic case on the boundary of the EP transition to zero on the instability threshold (Fig. 3). Thus in every case, this oscillation amplitude is always below the elastic limit for  $\tau \geq \tau_m$  and therefore it remains in the elastic regime.

One can also see that two kinds of unstable solutions exist. One corresponds to the cases that are also unstable for perfectly elastic solids ( $\hat{\lambda} \geq 1$ ) but the behavior changes after the amplitude have grown sufficiently to reach the plastic regime:

$$z(\tau) = \begin{cases} \frac{\hat{\lambda}}{\hat{\lambda}-1} (\cos \gamma' \tau - 1), & \tau \leq \tau_p \\ \frac{1}{\hat{\xi}} - 1 + \frac{C^2 e^{-(\tau-\tau_p)}}{2\hat{\xi}(u_p + \sqrt{u_p^2 - C^2})} + \frac{(u_p + \sqrt{u_p^2 - C^2}) e^{(\tau-\tau_p)}}{2\hat{\xi}}, & \tau \geq \tau_p, \end{cases} \quad (34)$$

where

$$\gamma' = \sqrt{\frac{\hat{\lambda} - 1}{\hat{\lambda}}}. \quad (35)$$

The second kind of unstable solutions corresponds to cases that are stable for perfectly elastic solids ( $\hat{\lambda} < 1$ ) but that are beyond the instability threshold ( $C^2 \leq 0$ ):

$$z(\tau) = \begin{cases} \frac{\hat{\lambda}}{1 - \hat{\lambda}}(1 - \cos \gamma\tau), & \tau \leq \tau_p \\ \frac{1}{\hat{\xi}} - 1 + \frac{C^2 e^{-(\tau - \tau_p)}}{2\hat{\xi}(u_p + \sqrt{u_p^2 - C^2})} + \frac{(u_p + \sqrt{u_p^2 - C^2})e^{(\tau - \tau_p)}}{2\hat{\xi}}, & \tau \geq \tau_p. \end{cases} \quad (36)$$

It is seen from Eqs. (34) and (36), that despite the different initial path, both kinds of unstable solutions have the same asymptotic behavior for  $\tau \rightarrow \infty$ :

$$\frac{\xi}{\xi_0} \rightarrow \frac{(u_p + \sqrt{u_p^2 - C^2})e^{-\tau_p}}{2\hat{\xi}} e^{\tau} = \frac{\xi_0^{eff}}{\xi_0} e^{\tau}. \quad (37)$$

This means that asymptotically, the unstable solutions yield an amplitude growth rate equal to  $\sqrt{k g}$  that coincides with the one for an ideal fluid. The two kinds of unstable solutions are also shown in Fig. 2 [curves (d) and (e)]. The “effective” initial amplitude  $\xi_0^{eff}/\xi_0$  defined in the previous equation is a function of the parameters  $\hat{\xi}$  and  $\hat{\lambda}$  and it has been represented in Fig. 4 as a function of  $\hat{\lambda}$  for several values of  $\hat{\xi}$ . It is seen that we always have  $\xi_0^{eff}/\xi_0 \leq 1/2$  and for the asymptotic unstable solutions, the amplitude grows

exponentially as if initially the perturbation would have been less than  $\xi_0$ .

### III. 2D NUMERICAL SIMULATIONS

For the completion of our study we have performed extensive 2D numerical simulations using the finite element code ABAQUS [41]. We have considered a plate with periodic symmetry boundaries at the edges in order to model a plate in plane strain of infinite lateral extent. On the other hand, we have taken the plate with a thickness  $h = 18.8$  mm which is large in comparison with the inverse of the wave numbers  $k^{-1}$ . This means that we consider  $kh \gg 1$  so that, to the end of studying the development of hydrodynamic instabilities the plate behaves like a half-space. In addition, we have adopted a Mie-Grüneisen EOS with a coefficient  $\Gamma = \rho_0 \Gamma_0 / \rho$ , where  $\Gamma_0$  is a parameter characteristic of the solid material and  $\rho_0$  is the mass density under normal conditions. We have also assumed the usual linear relationship between the shock velocity  $v_s$  and the particle velocity  $v_p$ :  $v_s = c_0 + s v_p$ , where  $c_0$  and  $s$  are characteristic constants of the material. Furthermore, we have considered two sets of values for those parameters corresponding, respectively, to aluminum ( $\rho_0 = 2.7$  g/cm<sup>3</sup>,  $s = 1.337$ ,  $\Gamma_0 = 2.16$ ,  $c_0 = 5380$  m/s) and to tungsten ( $\rho_0 = 19.3$  g/cm<sup>3</sup>,  $s = 1.237$ ,  $\Gamma_0 = 1.54$ ,  $c_0 = 4030$  m/s). Nevertheless, regarding the values of  $c_0$ , we have taken a value  $c'_0 \sim 10c_0$  in order to assure incompressibility [17]. As in Ref. [8], the values of the shear modulus  $G$  and the yield strength  $Y$  were taken as independent constants so that the effect of varying each parameter independently can be seen more clearly. In the same manner the driving pressure  $p_0$ , the initial perturbation amplitude  $\xi_0$  and the perturbation wavelength  $\lambda$  were varied in order to span the complete range of values of  $\hat{\xi}$  and  $\hat{\lambda}$  between 0 and 1 (see Table I). On the other hand, in order to have RTI as pure as possible, we first accelerate the uniform plate by using a uniform pressure that ramps linearly from the time  $t = -t_0$  up to the time  $t = 0$  when the pressure reaches its maximum value  $p_0$ . For  $t \geq 0$  the pressure at the plate surface is held constant and equal to  $p_0 + \delta p$ , where  $\delta p = -p_0(\xi_0/h)\sin kx$  is the initial asymmetry introduced to seed the instability once the plate has been uniformly accelerated.

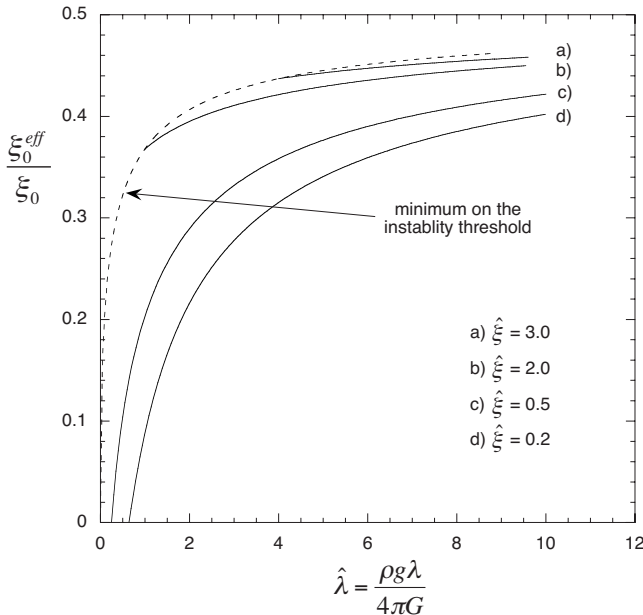


FIG. 4. Asymptotic dimensionless amplitude  $\xi_0^{eff}/\xi_0$  as a function of the dimensionless wavelength  $\hat{\lambda}$  for several values of the dimensionless amplitude  $\hat{\xi}$ .

TABLE I. Simulation data.  $h=18.8$  mm;  $p_0=\rho gh$ .

$\rho g \lambda / 4 \pi G$	$\lambda$ (mm)	$G$ (MPa)	$Y_{TH}$ (MPa)	$Y_{EP}$ (MPa)	$\xi_0$ ( $\mu\text{m}$ )	$p_0$ (GPa)
$\rho=2.7$ g/cm <sup>3</sup>						
0.055	1.304	140.0	2.8		50	1.4
0.110	2.607	140.0	12.5	19.5	200	1.4
0.150	2.607	1030.0	72.0	104.0	100	14.0
0.190	2.607	80.0	15.5	21.5	200	1.4
0.240	6.642	1640.0	42.0	59.0	50	14.0
0.280	6.642	140.0	18.5	23.5	200	1.4
0.350	9.406	1600.0	52.5	66.0	50	14.0
0.400	9.406	140.0	23.0	28.5	200	1.4
0.450	9.406	1240.0	62.5	81.5	50	14.0
0.490	6.642	80.0	21.5	26.5	150	1.4
0.550	12.875	140.0	32.0	40.5	200	1.4
0.600	12.875	1277.0	102.5	105.0	50	14.0
0.650	12.875	1170.0	122.5	122.5	50	14.0
0.700	9.406	80.0	57.0	57.0	200	1.4
0.750	9.406	746.0	172.5	172.5	50	14.0
0.800	18.812	140.0	23.0	23.0	50	1.4
0.850	9.406	658.0	335.0	335.0	50.0	14.0
0.890	12.014	80.0	48.0	48.0	50	1.4
0.930	22.046	140.0	20.5	20.5	10	1.4
$\rho=19.3$ g/cm <sup>3</sup>						
0.082	2.607	1350.0	20.5	35.5	50	10
0.310	6.642	911.0	35.0	43.5	200	10
0.520	6.642	543.0	53.0	64.0	50	10
0.870	12.134	587.4	250.0	250.0	50	10

Because of the plate incompressibility, this asymmetry immediately diffuses toward the plate interior. With  $t_0=15 \mu\text{s}$  we get a very uniform and constant acceleration for the two sets of  $p_0$  values considered in our study (Table I).

For the numerical simulation study of the instability threshold we have varied the parameters in order to meet the conditions for marginal stability following a procedure similar to the one described in Ref. [8]. These values have been represented in Fig. 1 together with the results of the analytic model. The two are in excellent agreement. In Fig. 1 we have also represented the numerical results that determine the boundary for the EP transition. For the latter, we have looked at the values of  $\hat{\xi}$  for fixed values of  $\hat{\lambda} < 1$  from which the amplitude of the elastic oscillations (for  $\tau \geq \tau_m$ ) starts to deviate from the perfectly elastic case. The values of all the parameters corresponding to the dots represented in Fig. 1 for the instability threshold and for the EP transition boundary are given in detail in Table I.

We have also calculated the maximum perturbation amplitude  $\xi_m^{TH}$  just on the instability threshold in order to compare it with the results given by Eqs. (30) and (31). The results are shown in Fig. 5 together with the analytic curve given by the model. In the same figure, we have also represented the Drucker criterion for comparison. As is seen, the Drucker criterion approximately applies to relatively short

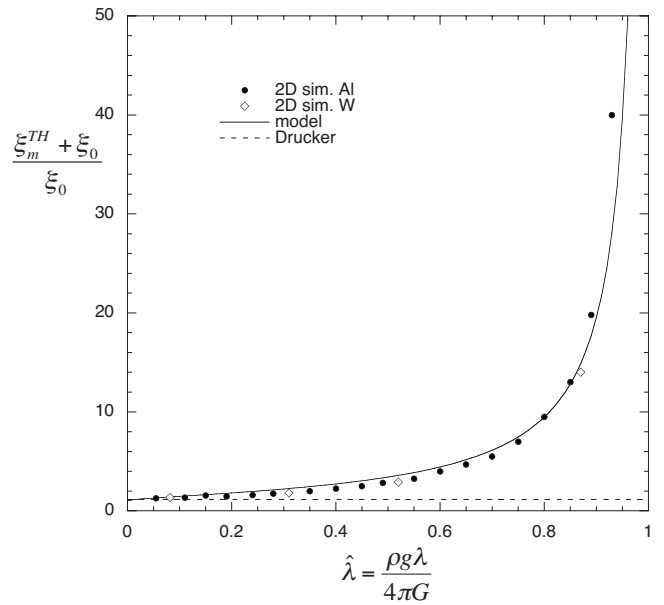


FIG. 5. Maximum perturbation amplitude  $\xi_m^{TH}$  on the instability threshold as a function of the dimensionless perturbation wavelength  $\hat{\lambda}$ . The full line is given by the analytic model and dots are obtained from ABAQUS 2D numerical simulations for Al and W. The dotted line shows the Drucker criterion.

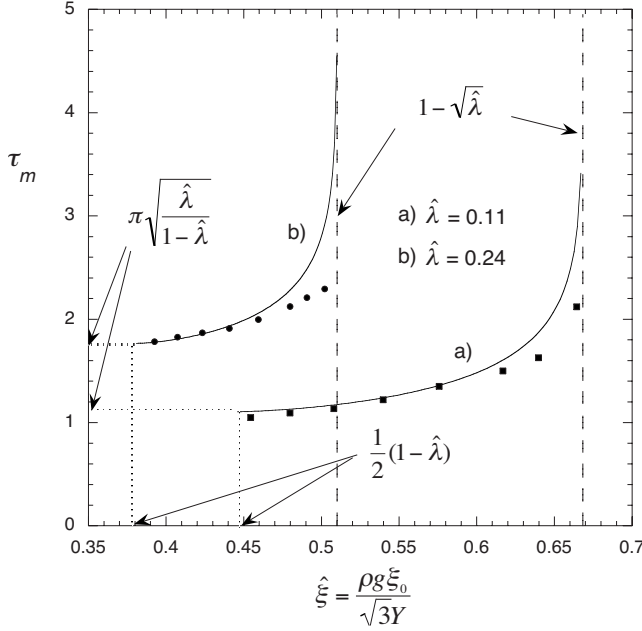


FIG. 6. Dimensionless time  $\tau_m$  of maximum amplitude of the stable cases as a function of the dimensionless initial perturbation amplitude  $\hat{\xi}$  for different values of the dimensionless perturbation wavelength  $\hat{\lambda}$ . Dots are given by the 2D numerical simulations for aluminum plates. Full lines are given by the model.

wavelengths (see also Fig. 1), or more precisely, to values of  $\hat{\lambda} \leq 0.2$ .

In Fig. 6 we have presented the dimensionless time  $\tau_m$  at which the stable solutions reach the maximum amplitude (see also Fig. 2) as a function of the dimensionless initial perturbation amplitude  $\hat{\xi}$  for different values of the dimensionless perturbation wavelength  $\hat{\lambda}$ . Dots are given by the numerical simulations for aluminum plates and the curves are calculated with the analytic model using Eq. (33). For a fixed value of  $\hat{\lambda}$ , the time  $\tau_m$  varies from the minimum  $\tau_m^{EP} = \pi\sqrt{\hat{\lambda}/(1-\hat{\lambda})}$  on the boundary of the EP transition (which corresponds to the half of the period of the elastic oscillations) to infinite on the instability threshold (where the amplitude  $A$  of the elastic oscillations tends to zero).

In Fig. 7 we show the maximum amplitude  $\xi_m$  of the perturbation reached at the time  $\tau_m$  (see Fig. 2) as a function of the dimensionless initial perturbation amplitude  $\hat{\xi}$  for the same values of the dimensionless perturbation wavelength  $\hat{\lambda}$  as in Fig. 6. Dots correspond to the numerical simulations for the same cases as in Fig. 6. We can see that the maximum perturbation amplitude  $\xi_m$  varies from a minimum for which we have  $(\xi_m^{EP} + \xi_0)/\xi_0 = (1+\hat{\lambda})/(1-\hat{\lambda})$  on the boundary for the EP transition and corresponding to the maximum amplitude of oscillation for a perfectly elastic solid to the maximum value for which  $(\xi_m^{TH} + \xi_0)/\xi_0 = 1/(1-\sqrt{\hat{\lambda}})$  and it is reached on the instability threshold (see also Fig. 5).

Numerical simulations also show that, asymptotically, the unstable evolutions of the perturbation amplitude grow exponentially with a growth rate equal to  $\sqrt{kg}$ , in agreement with Eq. (37), for  $\hat{\lambda} < 1$  as well as  $\hat{\lambda} > 1$ . The latter case takes

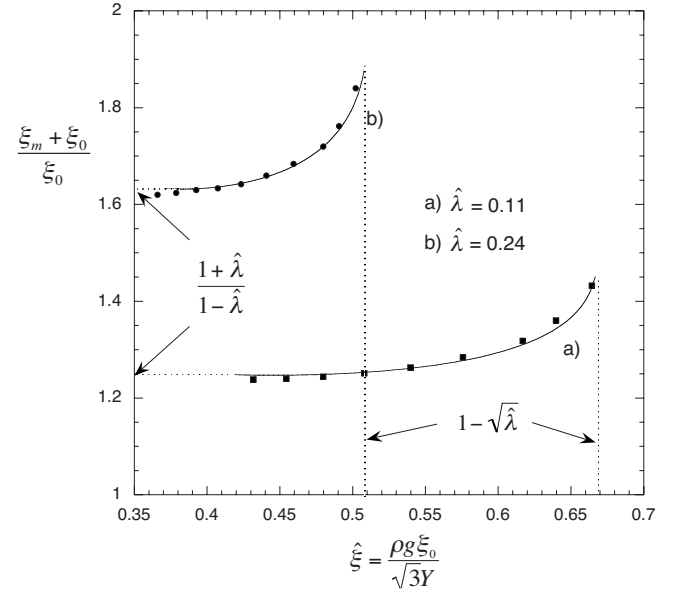


FIG. 7. Maximum amplitude  $\xi_m$  of the perturbation as a function of the dimensionless initial perturbation amplitude  $\hat{\xi}$  for the same values of the dimensionless perturbation wavelength  $\hat{\lambda}$  than in Fig. 6. Dots correspond to the numerical simulations for the same cases as in Fig. 6.

a somewhat longer time to reach the asymptotic behavior after it goes through a phase with the characteristic growth rate of an elastic solid [35–37].

With the aim to check the effect of the compressibility, we have also performed numerical simulations with relatively small values of the EOS parameter  $c_0$ . As it also happens in gas dynamics, these compressibility effects are not yet well understood [50–52] and since a systematic analysis is beyond the scope of the present work, it will require further investigation in the future. Nevertheless, the present numerical simulations indicate clearly a reduction of the instability threshold that is stronger as the compressibility increases (by decreasing  $c_0$ ) in such a manner that the incompressible boundary given by Eq. (27) represents to an upper limit for the instability threshold. Here we can only speculate that a possible reason for these results is that as the sound speed is reduced, the instability affects a region of the plate of size smaller than  $k^{-1}$ . Then, the system has less inertia and it becomes more unstable.

#### IV. CONCLUDING REMARKS

We have performed the linear analysis of the incompressible RTI in thick elastic-plastic plates accelerated uniformly by a constant pressure. For this purpose, we have used a relatively simple model that allows for dealing with the complex conditions arising from the nonlinear constitutive equations that model the behavior of elastic-plastic solids.

The model allows for obtaining explicit analytical solutions for the evolution of the perturbation amplitude. These solutions are characterized by two-dimensionless parameters, namely, the dimensionless initial perturbation amplitude  $\hat{\xi}$

and the dimensionless perturbation wavelength  $\hat{\lambda}$ . Depending on the values of these parameters we can identify four different kinds of evolutions. There are two stable solutions for  $\hat{\lambda} < 1$ : one for  $\hat{\xi} \leq (1 - \hat{\lambda})/2$  the other one for  $(1 - \hat{\lambda})/2 \leq \hat{\xi} \leq 1 - \sqrt{\hat{\lambda}}$ . The other two solutions are unstable and one corresponds to  $\hat{\lambda} < 1$  and  $\hat{\xi} > 1 - \sqrt{\hat{\lambda}}$  and the other one to  $\hat{\lambda} > 1$  (Fig. 2). Stable and unstable solutions are separated by the instability threshold given by Eq. (26). These results as well as quantitative values of the relevant parameters characterizing the perturbation evolution has been compared with extensive 2D numerical simulations performed with the code ABAQUS and the results are found to be in excellent agreement.

Both, the model and the simulations show that for  $\hat{\lambda} < 1$  the EP transition must always occur before the instability threshold is achieved. This demonstrates clearly that the achievement of the elastic limit is not a sufficient condition for instability as it was supposed in the past.

The present results have direct implications on the design of experiments on HEDP. For the particular case of the LAPLAS experiment in which we are interested, Eq. (27) helps to make the best choice for pusher materials in the cylindrical shell target. In fact, to assure stabilizing effects from the constitutive properties of the pusher material we must require, at least, that  $Y > (p_0/\sqrt{3})(\xi_0/h)$ . In the LAPLAS experiment the asymmetry level will be essentially determined by the wobbler system producing the beam rotation for heating the annular absorber region. For a typical parabolic power pulse the asymmetry level  $\xi_0/h$  has been shown to be  $\xi_0/h = 1/N^2$ , where  $N$  is the number of revolutions of the beam during the pulse duration  $\tau_{\text{beam}}$  [24,25]. At present, FAIR is designed to deliver pulses with  $\tau_{\text{beam}} \approx 100$  ns and the wobbler system is being designed to generate more than 30 revolutions during this pulse duration [53]. Thus,  $\xi_0/h \approx 10^{-3}$ . For driving pressures in the range of 1 to 10 Mbar we need  $Y > 0.06 - 0.6$  GPa. The materials considered so far for LAPLAS have been gold and lead because of their high densities ( $\rho_{\text{Au}} = 19.3$  g/cm<sup>3</sup>;  $\rho_{\text{Pb}} = 11.3$  g/cm<sup>3</sup>). According to Ref. [54] the maximum values of  $Y$  reported in the literature for gold and lead are, respectively, 0.225 and 0.1 Gpa, what may make them not very suitable materials for LAPLAS from the point of view of the implosion stability. Better choices would be tungsten and tantalum which have similar densities ( $\rho_{\text{W}} = 19.3$  g/cm<sup>3</sup>;  $\rho_{\text{Ta}} = 16.7$  g/cm<sup>3</sup>) but have higher values of  $Y$ :  $Y_{\text{W}} = 2.2 - 4$  GPa and  $Y_{\text{Ta}} = 0.77 - 1$  GPa, besides of having the highest melting temperatures and high values of  $G$ :  $G_{\text{W}} = 160$  GPa and  $G_{\text{Ta}} = 69$  GPa [54].

In conclusion, although the model based on the Newton second law may constitute a rather simple approximation to the complex physics present in the evolution of the RTI in solids, it has been shown that the model is able to describe the essential features very accurately. In particular, for the present problem of elastic-plastic materials, the excellent agreement with the 2D numerical simulations confirms the physically intuitive expectation that the instability is not controlled by the details of the behavior of a material point but rather it is governed by the bulk motion of the mass con-

tained within the region with a thickness  $k^{-1}$ . It is for this global region that we can apply the Newton second law thus avoiding the local complexities of the deviatoric part  $S_{ij}$  of the stress tensor perturbation [48]. In this sense the approximated expression for  $S_{ij}$  given by Eq. (18) should not be intended as a representation of the actual stress spatial distribution but rather as a description of the average value on the region affected by the instability. In fact this is all we can get by assuming the simplest perturbed velocity field given by Eq. (3) but it is sufficient for describing the bulk motion of the mass affected by the instability. Certainly the construction of a complete self-consistent theory able to capture all the complexities of the local behavior of  $S_{ij}$  and of the exact velocity field may shed light on the phenomena underlying RTI in solids but for now such a theory continues presenting a challenge that seems to be beyond our present capabilities. In any case, the results presented here may indicate a way to get around to such a challenge.

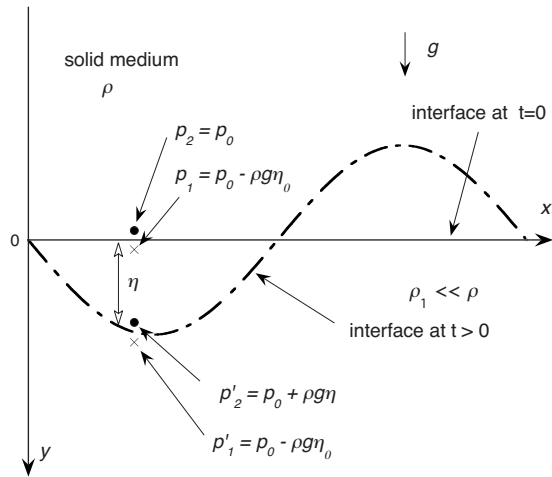
## ACKNOWLEDGMENTS

The authors wish to thank to G. Wouchuk and A. Ng for very helpful discussions and comments. This work has been partially supported by the Ministerio de Ciencia y Tecnología (Grant No. FIS2006-05389) and by the Consejería de Ciencia y Tecnología of Spain (Grants No. PAI08-0152-7994 and No. PAI08-0162-9026) and by the BMBF of Germany, and it has been performed under the International Atomic Energy (IAEA) Agreement No. 13820/R0.

## APPENDIX: EQUATION OF MOTION

Equation (1) is essentially the same as Eq. (5) in Ref. [37] and as Eq. (8) in Ref. [38]. (see also Eq. (5) in Ref. [39]) where an initially corrugated interface under the action of a perfectly uniform driving pressure was considered. However, may be of interest to rederive it here for our present case in which a thick plate ( $kh \gg 1$ ), perfectly planar at  $t=0$ , is accelerated by a nonuniform pressure consisting in a uniform pressure  $p_0 = \rho gh$  with a superposed ripple  $\delta p = -\rho g \xi_0 e^{ky} \sin kx$ .

Let us first consider a plate made of an ideal fluid of density  $\rho$  that is accelerated by the pressure  $p = p_0 + \delta p$ . Then, at  $t=0$  the pressure of the fluid elements lying immediately above the interface is  $p_2 = p_0$  and the pressure below the interface is  $p_1 = p_0 - \rho g \eta_0$  ( $\eta_0 = \xi_0 e^{ky} \sin kx$ ), so that a pressure difference  $\Delta p = \delta p = \rho g \eta_0$  exists at  $t=0$  (see Fig. 8). At times  $t > 0$  the interface undergoes a deformation  $\eta(x, y, t)$  given by Eq. (4) and at the new position the pressure of the fluid elements above the interface becomes  $p'_2 = p_0 + \rho g \eta$ . That is, the pressure increases at the valleys since these elements are now in a deeper place within the fluid (Fig. 8). In the same manner pressure decreases at the crests. On the other hand, pressure remains the same below the interface:  $p'_1 = p_1 = p_0 - \rho g \eta_0$  and, therefore, the pressure difference across the interface at  $t > 0$  becomes  $\Delta p' = \rho g (\eta + \eta_0)$ . This pressure difference drives the motion of the interface according to the Newton second law:


 FIG. 8. Schematic of the interface at  $t=0$  and at  $t>0$ .

$$m\ddot{\eta} = \Delta p' A, \quad (\text{A1})$$

where  $A$  is the area of the interface and  $m$  is the mass of the fluid involved in the motion due to the instability. Since in RTI we have to deal with surface modes that decay exponentially as  $e^{ky}$  ( $y < 0$ ), we can assume that in the linear regime only the fluid within a distance  $k^{-1}$  participates in the motion.

Then,  $m = \rho A/k$  and the equation of motion reads

$$\frac{\rho}{k} \ddot{\eta} = \rho g (\eta + \eta_0). \quad (\text{A2})$$

As it is well known, this equation yields the linear evolution of the classical RTI in an ideal fluid. If the fluid is not ideal and we neglect surface tension, the other forces that will be present on the interface and have to be included into the Newton second law are just the forces described by the perturbation of the deviatoric part  $S_{ij}$  of the stress tensor  $\sigma_{ij} = -p\delta_{ij} + S_{ij}$ . Thus, if  $S_{yy}$  and  $S_{yx}$  are the perturbation of the vertical components of  $S_{ij}$ , the vertical force  $f_y$  per unit of area that must be added in Eq. (A2) is

$$f_y = -S_{yy}n_y - S_{yx}n_x, \quad (\text{A3})$$

where  $n_i$  is the  $i$ th component of the unit vector  $\mathbf{n}$  directed outward along the normal to the interface. In the linear regime is  $n_x \sim k\xi \ll 1$  and  $n_y \approx 1$  so that the last term is negligible and the equation of motion turns out:

$$\frac{\rho}{k} \ddot{\eta} = \rho g (\eta + \eta_0) - S_{yy}. \quad (\text{A4})$$

This equation can be further generalized for including surface tension or a mass flux across the interface [37–39].

- 
- [1] Lord Rayleigh, *Scientific Papers* (Dover, New York, 1965), Vol. 2.
- [2] G. I. Taylor, Proc. R. Soc. London, Ser. A **201**, 192 (1950).
- [3] J. W. Miles, General Dynamics Report No. GAMD-7335, AD 643161, 1966 (unpublished).
- [4] G. N. White, Los Alamos National Laboratory Report No. LA-5225-MS, 1973 (unpublished).
- [5] J. F. Barnes, P. J. Blewett, R. G. McQueen, K. A. Meyer, and D. Venable, J. Appl. Phys. **45**, 727 (1974).
- [6] J. F. Barnes, D. H. Janney, R. K. London, K. A. Meyer, and D. H. Sharp, J. Appl. Phys. **51**, 4678 (1980).
- [7] J. K. Dienes, Phys. Fluids **21**, 736 (1978).
- [8] J. W. Swegle and A. C. Robinson, J. Appl. Phys. **66**, 2838 (1989).
- [9] A. C. Robinson and J. W. Swegle, J. Appl. Phys. **66**, 2859 (1989).
- [10] D. C. Drucker, in *Mechanics Today*, edited by S. Nemat-Nasser (Pergamon, Oxford, 1980), Vol. 5, p. 37.
- [11] D. C. Drucker, Ing.-Arch. **49**, 361 (1980).
- [12] E. L. Ruden and D. E. Bell, J. Appl. Phys. **82**, 163 (1997).
- [13] G. Dimonte, R. Gore, and M. Schneider, Phys. Rev. Lett. **80**, 1212 (1998).
- [14] G. Dimonte, Phys. Plasmas **6**, 2009 (1999).
- [15] P. N. Nizovtzev and P. N. Raevskii, Kvantovaya Elektron. (Kiev) **3**, 11 (1991).
- [16] A. I. Lebedev, P. N. Nizovtzev, P. N. Raevskii, and V. P. Solov'ev, Phys. Dokl. **41**, 328 (1996).
- [17] S. M. Bakhrakh, O. B. Drennov, N. P. Kovalev, A. I. Lebedev, E. E. Meshkov, A. L. Mikhailov, N. V. Neumerzhitsky, P. N. Nizovtzev, V. A. Rayevsky, G. P. Simonov, V. P. Solov'ev, and I. G. Zhidov, Lawrence Livermore National Laboratory Report No. UCRL-CR-126710, 1997 (unpublished).
- [18] A. S. Khan and S. Huang, *Continuos Theory of Plasticity* (Wiley, New York, 1995).
- [19] W. F. Henning, Nucl. Instrum. Methods Phys. Res. B **214**, 211 (2004).
- [20] N. A. Tahir, D. H. H. Hoffmann, A. Kozyreva, A. Tauschwitz, A. Shutov, J. A. Maruhn, P. Spiller, U. Neuner, R. Bock, H. Juranek, and R. Redmer, Phys. Rev. E **63**, 016402 (2001).
- [21] N. A. Tahir, H. Juranek, A. Shutov, R. Redmer, A. R. Piriz, M. Temporal, D. Varentsov, S. Udrea, D. H. H. Hoffmann, C. Deutsch, I. Lomonosov, and V. E. Fortov, Phys. Rev. B **67**, 184101 (2003).
- [22] A. R. Piriz, R. F. Portugues, N. A. Tahir, and D. H. H. Hoffmann, Phys. Rev. E **66**, 056403 (2002).
- [23] A. R. Piriz, R. F. Portugues, N. A. Tahir, and D. H. H. Hoffmann, Laser Part. Beams **20**, 427 (2002).
- [24] A. R. Piriz, N. A. Tahir, D. H. H. Hoffmann, and M. Temporal, Phys. Rev. E **67**, 017501 (2003).
- [25] A. R. Piriz, M. Temporal, N. A. Tahir, and D. H. H. Hoffmann, Plasma Phys. Contr. Fusion **45**, 1733 (2003).
- [26] R. E. Reinovsky, W. E. Anderson, W. L. Atchison, C. E. Ekdahl, R. J. Faehl, I. R. Lindemuth, D. V. Morgan, M. Murillo, J. L. Stokes, and J. S. Shlachter, IEEE Trans. Plasma Sci. **30**, 1764 (2002).
- [27] J. W. Shaner, Physica D **12**, 154 (1984).
- [28] D. H. Kalantar, B. A. Remington, J. D. Colvin, K. O. Mikaelian, S. V. Weber, L. G. Wiley, J. S. Wark, A. Loveridge, A. M.

- Allen, A. A. Hauer, and M. A. Meyers, *Phys. Plasmas* **7**, 1999 (2000).
- [29] K. T. Lorenz, M. J. Edwards, S. G. Glendinning, A. F. Janakowsky, J. McNaney, S. M. Pollaine, and B. A. Remington, *Phys. Plasmas* **12**, 056309 (2005).
- [30] B. A. Remington, P. Allen, E. M. Bringa, J. Hawreliak, D. Ho, K. T. Lorenz, H. Lorenzana, J. M. McNaney, M. A. Meyers, S. W. Pollaine, K. Rosolankova, B. Sadik, M. S. Schneider, D. Swift, J. Wark, and B. Yaakobi, *Mater. Sci. Technol.* **22**, 474 (2006).
- [31] J. D. Colvin, M. Legrand, B. A. Remington, G. Shurtz, and S. V. Weber, *J. Appl. Phys.* **93**, 5287 (2003).
- [32] G. H. Houseman and P. Molnar, *Geophys. J. Int.* **128**, 125 (1997).
- [33] E. B. Burov and P. Molnar, *Earth Planet. Sci. Lett.* **275**, 370 (2008).
- [34] O. Blaes, R. Blandford, and P. Madau, *Appita J.* **363**, 612 (1990).
- [35] B. J. Plohr and D. H. Sharp, *Z. Angew. Math. Phys.* **49**, 786 (1998).
- [36] G. Terrones, *Phys. Rev. E* **71**, 036306 (2005).
- [37] A. R. Piriz, J. J. Lopez-Cela, O. D. Cortazar, N. A. Tahir, and D. H. H. Hoffmann, *Phys. Rev. E* **72**, 056313 (2005).
- [38] A. R. Piriz, O. D. Cortazar, J. J. Lopez-Cela, and N. A. Tahir, *Am. J. Phys.* **74**, 1095 (2006).
- [39] A. R. Piriz, J. J. Lopez Cela, M. C. Serna Moreno, N. A. Tahir, and D. H. H. Hoffmann, *Laser Part. Beams* **24**, 275 (2006).
- [40] A. R. Piriz, J. J. Lopez-Cela, and N. A. Tahir, *J. Appl. Phys.* **105**, 116101 (2009).
- [41] ABAQUS, *Finite Element Code, Version 6.6* (Hibbit, Kalsson and Sorensen, Pawtucket, RI, 2006).
- [42] J. G. Wouchuk, *Phys. Rev. E* **63**, 056303 (2001).
- [43] K. Nishihara, R. Ishizaki, J. G. Wouchuk, Y. Fukuda, and Y. Shimuta, *Phys. Plasmas* **5**, 1945 (1998).
- [44] A. R. Piriz, J. J. Lopez-Cela, N. A. Tahir, and D. H. H. Hoffmann, *Phys. Rev. E* **78**, 056401 (2008).
- [45] J. M. Clarisse, C. Boudesocque-Dubois, and S. Gauthier, *J. Fluid Mech.* **609**, 1 (2008).
- [46] R. Betti, V. Lobatchev, and R. L. McCrory, *Phys. Rev. Lett.* **81**, 5560 (1998).
- [47] G. K. Batchelor, *An Introduction to Fluid Mechanics* (Cambridge University Press, New York, 1973).
- [48] G. Terrones, *J. Appl. Phys.* **102**, 034908 (2007).
- [49] P. A. G. Scheuer, *J. Astrophys. Astron.* **2**, 165 (1981).
- [50] D. Livescu, *Phys. Fluids* **16**, 118 (2004); **17**, 069101 (2005); **17**, 089101 (2005).
- [51] X. Ribeyre, V. T. Tikhonchuk and S. Bouquet, *Phys. Fluids* **16**, 4661 (2004); **17**, 069102 (2005).
- [52] A. R. Piriz, *Phys. Plasmas* **8**, 5268 (2001).
- [53] A. Golubev (private communication).
- [54] D. J. Steinberg, S. G. Cochran, and M. W. Guinan, *J. Appl. Phys.* **51**, 1498 (1980).